JOURNAL OF MATERIALS SCIENCE 31 (1996) 4521–4532

Non-hookean stress–strain response and changes in crystallite orientation of carbon fibres

M. SHIOYA, E. HAYAKAWA, A. TAKAKU
Department of Organic and Polymeric Materials, Tokyo Institute of Technology, 2-12-1 O-okayama, Meguro-ku, Tokyo 152, Japan

The non-hookean stress–strain response of carbon fibres was investigated in relation to changes in crystallite orientation with tensile stress. Various one-dimensional array models and a mosaic model were examined. Amongst these models, only the mosaic model in which the stress of the crystallites can be transmitted in both the transverse and the axial directions showed any quantitative agreement with the measured increases in the tensile modulus and the crystallite orientation with tensile stress. This suggests that deformation of the crystallites is constrained with increasing tensile stress. It was also found that the ratio of the tensile stress of the fibre to that of the crystallites is close to the crystallite volume fraction rather than the ratio of the fibre density to the crystallite density.

1. Introduction

The tensile modulus of carbon fibres increases with an increasing tensile stress applied to the fibres [1–6]. This non-hookean stress–strain response has also been observed for carbon fibre products in various forms such as unidirectional composites [4, 7–12] and multidirectional laminates [13]. The non-hookean stress–strain response of carbon fibres is reversible [1, 14] and it is unaffected by the cycles of loading and unloading up to at least 40% of the tensile strength [5, 12]. This suggests that the non-hookean stress–strain response of carbon fibres is not due to either partial destruction of the fibre structure or plastic deformation of the materials.

In the case of polyacrylonitrile (PAN)-based carbon fibres the increase in tensile modulus with tensile stress tends to be higher for fibres with a higher initial tensile modulus. Also; the rate of increase in the tensile modulus normalized by the initial tensile modulus against tensile stress takes a constant value of about 0.1 GPa^{-1} independent of the initial tensile modulus [12].

Carbon fibres consist of an assembly of crystallites which are parallel stacks of carbon layers similar to graphite. However, the relative displacements of the carbon layers in the direction parallel to the layer plane are not as regular as in graphite. The stacking regularity depends on the starting materials and preparation conditions of the carbon fibres [15].

Graphite is mechanically anisotropic and its stiffness parallel to the layer plane is 1060 GPa while, the stiffness normal to the layer plane is only 36.5 GPa. As is expected from this mechanical anisotropy of graphite, the tensile modulus of carbon fibres strongly depends on the crystallite orientation. Generally, carbon fibres with a higher orientation of the carbon layers in the direction of the fibre axis develop a higher tensile modulus.

The crystallite orientation of carbon fibres also changes with tensile stress applied to the fibres [1] and increases with increasing tensile stress. The rate of increase in the crystallite orientation with tensile stress tends to be higher for fibres having lower initial crystallite orientation [16]. Thus the tensile stress dependencies of the tensile modulus and the crystallite orientation, found for specified carbon fibres, are expected to be consistent with the relationships between the initial tensile modulus and the initial crystallite orientation observed amongst carbon fibres of different types. However, a functional relation between the tensile modulus and the crystallite orientation at various stresses differs from that found between the initial tensile modulus and the initial crystallite orientation for various carbon fibres [14]. This implies that the crystallite orientation is not a decisive factor determining the tensile modulus of carbon fibres.

Various mechanical models of carbon fibres have been proposed in order to explain the relationships between the tensile modulus and the crystallite orientation [6, 17, 18]. However, it has not yet been verified whether or not these proposed models can explain the stress–strain response associated with changes in the crystallite orientation with tensile stress.

In the present study, the changes of the tensile modulus and the crystallite orientation with tensile stress for carbon fibres have been analysed on the basis of a detailed experimental investigation. The various mechanical models currently available have been critically examined and a new model is proposed.

2. Stress–strain response and orientation changes

2.1 Preparation of composite specimens

Commercial PAN-based carbon fibres with various tensile moduli were used for the experiments. These

0022–2461

fibres were in the form of tow comprising 2000–12 000 filaments depending on the specific fibre type.

The measurement of the stress–strain response and the X-ray diffraction were made on carbon fibre/epoxy resin unidirectional composite strands under tensile stress. A resin system comprising 49.9 parts by weight (p.b.w.) diglycidil ether of bisphenol A type epoxy resin, 49.9 p.b.w. 4-methyl hexahydrophthalic acid anhydride and 0.2 p.b.w. 1-butyl-2-methylimidazole were used as the matrix. A carbon fibre tow was first soaked in the resin, and passed through a circular die in order to squeeze out any excess resin. Then the resin impregnated tow was cured at 110 °C for 1 h and then post-cured at 150 °C for 3 h. The volume fraction of carbon fibres in a composite strand was about 0.6.

2.2 Stress–strain response

The stress–strain response of composite strands was measured with a tensile tester equipped with pneumatically actuated clamps. The gauge length of the specimen was 100 mm, and the cross head speed was 0.5 mm min^{-1}. The elongation of the specimen was measured with a clip-on extensometer. The force–elongation signals were recorded at a time interval of 50 ms with a microcomputer.

The tensile stress of the carbon fibres in a composite strand was calculated by dividing the tensile force applied to the composite strand by the cross-sectional area of the carbon fibres in the composite strand, ignoring a small force supported by the matrix resin. The cross-sectional area of the carbon fibres in the composite strand was calculated from the mass per unit length and the density of the carbon fibres. The fibre density was determined by a sink-float method.

The tangent modulus E of carbon fibres was calculated from the stress–strain response according to the definition,

$$E = \left(\frac{\partial \varepsilon}{\partial \sigma}\right)^{-1} \quad (1)$$

where σ and ε are the tensile stress and the tensile strain of the carbon fibres, respectively. The changes of the tangent modulus with tensile stress for a series of PAN-based carbon fibres are shown in Fig. 1. Each data point is the average of five composite strands.

From Fig. 1, the tangent modulus at zero tensile stress was determined by extrapolating the changes in the tangent modulus at lower tensile stresses to zero tensile stress, since there is a possibility that the slight bending of the composite strand, when gripped with the pneumatically actuated clamps, could produce an inaccurate tangent modulus at start of tensile loading. These extrapolated values, as well as the succeeding tangent moduli under tensile stress, were consistent with tensile moduli determined in ultrasonic experiments [12].

2.3 Changes of orientation with tensile stress

The changes in the crystallite orientation with tensile stress were measured by using the 002 diffraction peak

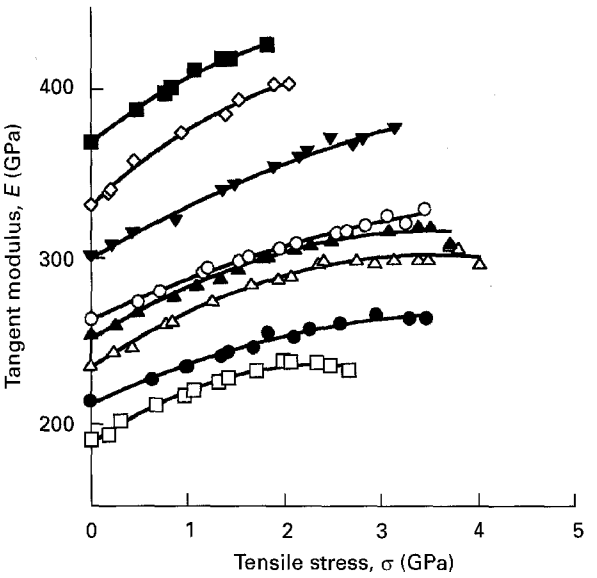

Figure 1 Tangent modulus E of PAN-based carbon fibres plotted against tensile stress σ of fibre. Different fibres are shown by different symbols.

with an X-ray diffraction apparatus attached to a tensile tester [16]. A pinhole-collimated and nickel-filtered CuK_α X-ray beam was incident perpendicularly on a composite strand held with pneumatically actuated clamps. The diffracted X-ray beam was detected with a linear position sensitive proportional counter (PSPC) through a metal arc-slit attached to the entrance window of the PSPC. In this manner, the intensity distribution, as a function of the azimuthal angle, of the 002 diffraction peak was measured at desired time intervals while stretching a specimen at a cross head speed of 0.5 mm per min. The gauge length of the specimen was 100 mm.

In the case of carbon fibres with a high crystallite orientation such as those used in the present study, the distribution density function $g(\xi)$ of the orientation angle ξ between the normal of the carbon layer and the fibre axis can be closely approximated by an orientation distribution function of the form [16]

$$g(\xi) = K \sin^{\omega}\xi \quad (2)$$

where

$$K = \frac{\Gamma\left(\frac{\omega+3}{2}\right)}{2\pi^{3/2}\Gamma\left(\frac{\omega+2}{2}\right)} \quad (3)$$

$$\omega = -\frac{\ln 2}{\ln\left(\cos\left[\frac{\Delta\xi}{2}\right]\right)} \quad (4)$$

$\Delta\xi$ is the full-width at half-maximum of $g(\xi)$, and $\Gamma(x)$ is a gamma function having the following property

$$\Gamma(x+1) = x\Gamma(x) \quad (\text{real } x > 0) \quad (5)$$

By defining $\langle p \rangle$ as the average of an arbitrary parameter p with respect to the orientation distribution function, the orientation distribution function is normalized such that

$$\langle 1 \rangle = 1 \quad (6)$$

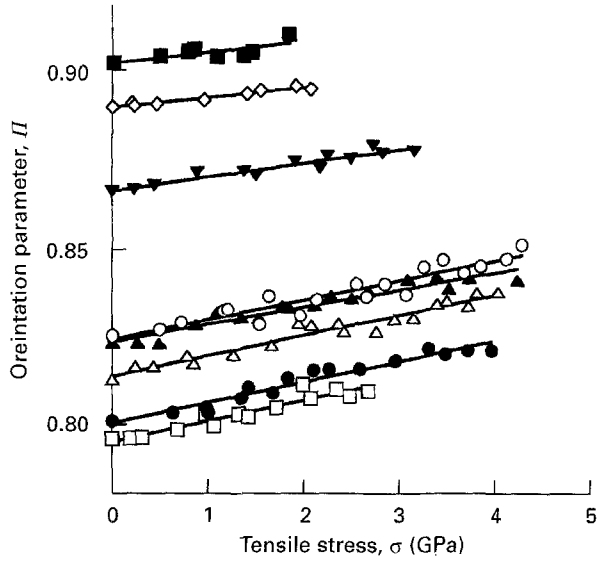

Figure 2 Orientation parameter Π of PAN-based carbon fibres plotted against tensile stress σ of fibre. Symbols correspond to Fig. 1.

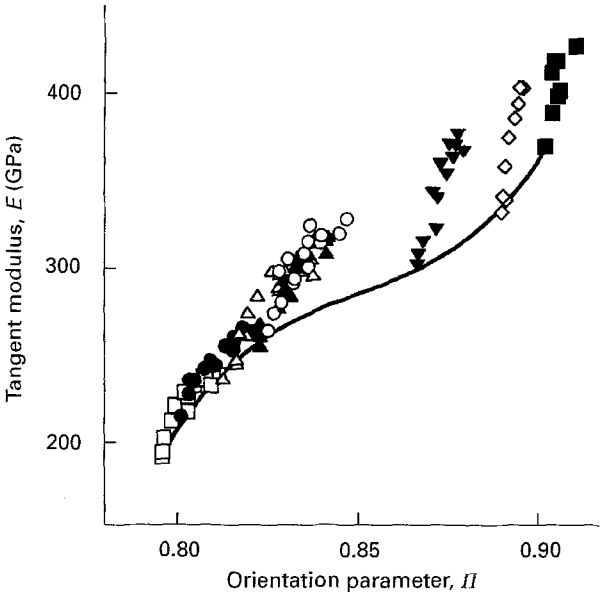

Figure 3 Tangent modulus E of PAN-based carbon fibres at various tensile stresses plotted against orientation parameter Π. The curve approximates the relation between initial tangent modulus and initial orientation parameter for various fibres. Symbols correspond to Fig. 1.

where

$$\langle p \rangle = \int_0^{\pi} 2\pi \sin\xi g(\xi) p \, d\xi \tag{7}$$

The average of $\sin^n \xi$ which often appears in later sections is calculated as

$$\langle \sin^n \xi \rangle = \frac{(\omega + 1)(\omega + n)}{\omega(\omega + n + 1)} \times \frac{\Gamma\left(\frac{\omega+1}{2}\right)\Gamma\left(\frac{\omega+n}{2}\right)}{\Gamma\left(\frac{\omega}{2}\right)\Gamma\left(\frac{\omega+n+1}{2}\right)} \tag{8}$$

In the present study, as an extent of the crystallite orientation, the orientation parameter Π defined as

$$\Pi = 1 - \frac{\Delta\xi}{\pi} \tag{9}$$

is used. By determining experimentally this orientation parameter, the orientation distribution function of Equation 2 is obtained according to the relations of Equations 3, 4 and 9 .

Fig. 2 shows the variation of the orientation parameter with tensile stress for a series of PAN-based carbon fibres. The relation between the crystallite orientation parameter Π and the tensile stress σ in GPa can be approximated by an empirical equation,

$$\Pi = 0.029(1 - \Pi_0)\sigma + \Pi_0 \tag{10}$$

where Π_0 is the crystallite orientation parameter at zero tensile stress [16].

On the basis of the tangent modulus versus tensile stress relation in Fig. 1 and the crystallite orientation versus tensile stress relation in Fig. 2 the tangent modulus is plotted against the crystallite orientation in Fig. 3. In Fig. 3, the continuous line represents the relation between the initial values of the tangent modulus and the crystallite orientation for carbon fibres of various types. Under tensile stress the tangent modulus increases with the crystallite orientation at a faster rate than observed in the relation between the initial values of the tangent moduli and the crystallite orientation.

3. One-dimensional array models for non-hookean stress–strain response with orientation changes

The mechanical models for explaining the relationships between the mechanical properties and structure may be classified into two types, one is a model comprised of a series combination of crystallites, and the other a parallel combination of crystallites. These models will be called one-dimensional array models in the sense that in these models the crystallites are arranged in a one-dimensional array.

3.1 One-dimensional array models

3.1.1 Undulating ribbon model

In the undulating ribbon model shown in Fig. 4, it is assumed that the parallel stack of ribbon-like carbon layers undulates in such a way that the normal vectors of the carbon layers at any position are coplanar. The configuration of undulation is determined so that the distribution of the layer normals coincides with the orientation distribution function. The undulating ribbon is comprised of a series combination of undulating elements which are constant in configuration and have an undulation of a unit cycle. Then the modulus of the whole undulating ribbon equals that of the undulating element. The undulating ribbon has a rectangular cross-section with the layer stacking height h and area A. Both the ends of the undulating ribbon are aligned in parallel to the fibre axis.

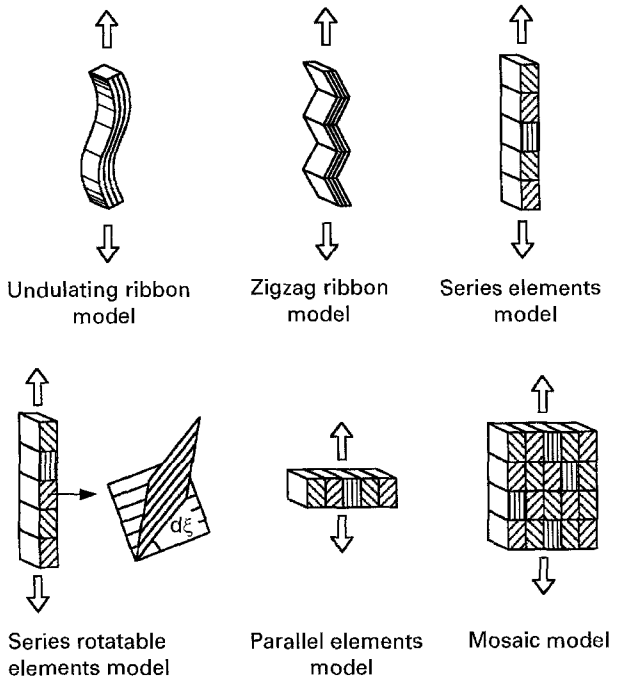

Figure 4 Schematic illustrations of undulating ribbon, zigzag ribbon, series elements, series rotatable elements, parallel elements and mosaic models.

The deformation of the undulating ribbon can be analyzed by using the theorem of Castigliano. Consider that the undulating ribbon is a perfectly elastic body subjected to a force F causing, at the loading point, a component of displacement z in the same direction as the applied force. If the elastic strain energy stored in the undulating ribbon is denoted by U, then the displacement is generally represented by

$$Z = \frac{\partial U}{\partial F} \tag{11}$$

If the height h is sufficiently smaller than a radius of curvature of the undulation, and if the shear force in the cross-section can be ignored, then an elastic strain energy dU stored in an element of length dL formed by two cross-sections is given by

$$dU = \frac{N^2 s_{11}}{2A} dL + \frac{M^2 s_{11}}{2I} dL \tag{12}$$

where N and s_{11} are respectively the force and the compliance normal to the cross-section, M the bending moment, and I the second moment of area of the cross-section.

Introduce a Cartesian coordinate (x, y) to the undulating element so that one end of the element locates on the origin and the other end aligns on the x-axis at $x = x_0$. The y-axis is arranged to be coplanar with the normal vectors of the carbon layers. The locus of the centreline of this element is represented by $y = f(x)$, and define the length L measured along the centreline to be zero at $x = 0$ and L_0 at $x = x_0$. The angle between a normal vector of the carbon layer and the x-axis is denoted by ξ.

When both ends of the undulating element are subjected to a tensile force F, the following relations are obtained.

$$N = \sin \xi F \tag{13}$$

$$M = f(x)F \tag{14}$$

$$I = \frac{Ah^2}{12} \tag{15}$$

Therefore, the tangent modulus E_f of the undulating ribbon is given by

$$\frac{1}{E_f} = \frac{d(z/x_0)}{d(F/A)} = \frac{s_{11}}{x_0} \int_0^{L_0} \left(\sin^2 \xi + \frac{12}{h^2} f^2 \right) dL \tag{16}$$

where ξ and dL can be related to x as

$$\sin^2 \xi = \frac{1}{(df/dx)^2 + 1} \tag{17}$$

$$dL = ((df/dx)^2 + 1)^{1/2} dx \tag{18}$$

It is assumed that ξ increases monotonically from zero to π as x increases from zero to x_0, and that the configuration of the undulating element has a mirror symmetry with respect to the plane $x = x_0/2$. Then a fractional length dL/L_0 having orientation angles between ξ and $\xi + d\xi$ is given by

$$\frac{dL}{L_0} = 2\pi \sin \xi \, g(\xi) \, d\xi \tag{19}$$

Hence, we have

$$x_0 = \int_0^{L_0} \sin \xi \, dL = \int_0^{\pi} 2\pi L_0 \sin^2 \xi \, g(\xi) \, d\xi \tag{20}$$

$$f = \int_0^{L} \cos \xi \, dL = \int_0^{\xi} 2\pi L_0 \sin \xi \cos \xi \, g(\xi) \, d\xi \tag{21}$$

Substituting these equations into Equation 16, and applying Equation 2 leads to the tangent modulus

$$\frac{1}{E_f} = \frac{(\omega + 2)^2}{2(\omega + 3)} \left\{ \frac{\Gamma\left(\frac{\omega + 2}{2}\right)}{\Gamma\left(\frac{\omega + 3}{2}\right)} \right\}^2 s_{11} + \left(\frac{L_0}{h}\right)^2 \frac{6}{\pi(\omega + 2)} \frac{\Gamma\left(\frac{\omega + 3}{2}\right)\Gamma\left(\frac{3\omega + 6}{2}\right)}{\Gamma\left(\frac{\omega + 2}{2}\right)\Gamma\left(\frac{3\omega + 7}{2}\right)} s_{11} \tag{22}$$

It is noted in Equation 12 that the cross-section of the undulating ribbon is assumed to be perpendicular to the centreline before and after deformation. This assumption may not hold if the compliance s_{44} for shear between carbon layers is sufficiently large. In the case where s_{44} is sufficiently large, the individual carbon layers deform independently without interacting with each other and the tangent modulus is calculated by an equation obtained by replacing h in Equation 22 with a thickness of a single carbon layer.

3.1.2. Zigzag ribbon model

In the zigzag ribbon model schematically shown in Fig. 4, it is assumed that the equidimensional crystallites are linked end to end to form a zigzag ribbon extending parallel to the fibre axis. Each crystallite is comprised of carbon layers stacked in parallel to a crystallite axis connecting two linking points at the ends of a crystallite. The normal of the carbon layers is in a plane defined by this crystallite axis and the fibre axis. The crystallite has a cross-sectional area A perpendicular to the crystallite axis, and the length of the crystallite axis is denoted as L.

When the tensile force F applied to both ends of this assembly of crystallites increases by dF, the crystallite is extended along the crystallite axis by dL. Simultaneously, the crystallite is rotated by an angle $d\xi$ in the plane defined by the crystallite axis and the fibre axis. The angle $d\xi$ is assumed to be proportional to the increment of the shear stress $d\sigma_{13}$ along the cross-section of the crystallite. That is,

$$dL = Ls_{11}\,d\sigma_{11} \tag{23}$$

$$d\xi = r_{55}d\sigma_{13} \tag{24}$$

where the suffix 1 represents the direction parallel to the layer plane, σ_{11} the tensile stress, s_{11} a component of the compliance matrix, and r_{55} a compliance for the rotation of the crystallite, relating the bending rigidity of the links or the resistance from surrounding materials. If $d\xi$ is proportional to the shear force then r_{55} is proportional to A, and if $d\xi$ is proportional to the bending moment at the links then r_{55} is proportional to LA.

The projection length of a crystallite onto the fibre axis is $\sin\xi L$. This projection length changes with the extension and the rotation of a crystallite by $\sin\xi\,dL$ and $\cos\xi\,L\,d\xi$, respectively. The whole projection length of the assembly equals the sum of the projection lengths of respective crystallites. Also, the extension of the assembly is given by the sum of the increments of the projection lengths of respective crystallites. Therefore, the strain ε_{ff} of the assembly is given by

$$d\varepsilon_{ff} = \frac{\langle \sin\xi\,dL + \cos\xi\,L\,d\xi\rangle}{\langle \sin\xi\,L\rangle} = \frac{\langle \sin\xi\,s_{11}\,d\sigma_{11} + \cos\xi\,r_{55}\,d\sigma_{13}\rangle}{\langle \sin\xi\rangle} \tag{25}$$

The area of a crystallite cross-sectioned perpendicularly to the fibre axis is $A/\sin\xi$. A crystallite with this cross-sectional area has a length of $\sin\xi L$ along the fibre axis. Hence, the average area A^* of the assembly cross-sectioned perpendicularly to the fibre axis is given by

$$A^* = \frac{\left\langle \frac{A}{\sin\xi}\sin\xi L\right\rangle}{\langle \sin\xi L\rangle} = \frac{A}{\langle \sin\xi\rangle} \tag{26}$$

By using the average area, the increment of an average tensile stress $d\sigma_{ff}$ is represented as

$$d\sigma_{ff} = \frac{dF}{A^*} = \frac{\langle \sin\xi\rangle}{A}dF \tag{27}$$

Thus,

$$d\sigma_{11} = \frac{\sin\xi\,dF}{A} = \frac{\sin\xi}{\langle \sin\xi\rangle}d\sigma_{ff} \tag{28}$$

$$d\sigma_{13} = \frac{\cos\xi\,dF}{A} = \frac{\cos\xi}{\langle \sin\xi\rangle}d\sigma_{ff} \tag{29}$$

Therefore, the tangent modulus E_f of the assembly is given by

$$\frac{1}{E_f} = \frac{d\varepsilon_{ff}}{d\sigma_{ff}} = \frac{\langle \sin^2\xi\rangle}{\langle \sin\xi\rangle^2}s_{11} + \frac{\langle \cos^2\xi\rangle}{\langle \cos\xi\rangle^2}r_{55} \tag{30}$$

By applying Equation 2,

$$\frac{1}{E_f} = \frac{\omega^4(\omega+2)^3}{4(\omega+1)^4(\omega+3)}\left\{\frac{\Gamma\left(\frac{\omega}{2}\right)}{\Gamma\left(\frac{\omega+1}{2}\right)}\right\}^4 \times\left(s_{11}+\frac{1}{\omega+2}r_{55}\right) \approx s_{11}+\frac{1}{\omega+2}r_{55} \tag{31}$$

The relation between the orientation angle and the tensile stress is obtained from Equations 24 and 29 as

$$\frac{d\xi}{\cos\xi} = \frac{r_{55}}{\langle \sin\xi\rangle}d\sigma_{ff} \approx r_{55}\,d\sigma_{ff} \tag{32}$$

Integrating the above equation leads to

$$\tan\left(\frac{\xi}{2}+\frac{\pi}{4}\right) = \tan\left(\frac{\xi_0}{2}+\frac{\pi}{4}\right)\exp(r_{55}\sigma_{ff}) \tag{33}$$

where ξ_0 is the initial orientation angle of a crystallite. When the assembly is subjected to tensile stress, the crystallites with orientation angles in a range from ξ_0 to $\xi_0+\partial\xi_0$ rotate into a range from ξ to $\xi+\partial\xi$. Simultaneously, the orientation distribution changes from the initial function $g_0(\xi_0)$ to $g(\xi)$. From the conservation in the number of crystallites,

$$2\pi\sin\xi_0\,g_0(\xi_0)\partial\xi_0 = 2\pi\sin\xi\,g(\xi)\partial\xi \tag{34}$$

Thus,

$$g(\xi) = \frac{\sin\xi_0}{\sin\xi}\frac{\partial\xi_0}{\partial\xi}g_0(\xi_0) \tag{35}$$

Differentiating Equation 33 with respect to ξ at a constant σ_{ff} gives

$$\frac{\partial\xi_0}{\partial\xi} = \exp(r_{55}\sigma_{ff}) \times\left\{\frac{\exp(-2r_{55}\sigma_{ff})-1}{\tan^2\left(\frac{\xi}{2}+\frac{\pi}{4}\right)\exp(-r_{55}\sigma_{ff})+1}+1\right\} \tag{36}$$

Therefore, the crystallite orientation at a stress σ_{ff} is obtained by using these equations. That is, the values of ξ_0 and $\partial\xi_0/\partial\xi$ are calculated by Equations 33 and 36 using the values of ξ and σ_{ff}. The value of $g_0(\xi_0)$ is

calculated by Equation 2 using the value of ξ_0. Then $g(\xi)$ is calculated by Equation 35, and the orientation parameter is obtained according to the definition of Equation 9.

3.1.3 Series elements model

In the series elements model shown in Fig. 4, the crystallites with a constant transverse cross-sectional area are combined in parallel to the fibre axis with a strong bond. Hence, when the assembly is subjected to a tensile stress, all the crystallites experience the same tensile stress.

Denote the length of the assembly by L, applied tensile stress by σ_{ff}, and resulting tensile strain by ε_{ff}. Then, the extension of the assembly $L\varepsilon_{ff}$ equals the sum of the extensions of respective crystallites. Since in an assembly the fractional length of crystallites with orientation angles from ξ to $\xi + d\xi$ is given by $2\pi \sin\xi\, g(\xi) L\, d\xi$, the extension of the assembly is expressed as

$$L\varepsilon_{ff} = \langle L s_{ff} \sigma_{ff} \rangle \tag{37}$$

In Equation 37, s_{ff} is the compliance in the fibre axis direction of a crystallite with an orientation angle ξ. This compliance is calculated by a coordinate transformation of the compliance matrix s_{ij} as

$$s_{ff} = (s_{11} - 2s_{13} + s_{33} - s_{44})\sin^4\xi + (2s_{13} - 2s_{33} + s_{44})\sin^2\xi + s_{33} \tag{38}$$

where the suffix 3 stands for the normal direction of the carbon layers, and the suffices 1 and 2 stand for the orthogonal directions in the layer plane. Therefore, by using Equation 2, the tangent modulus E_f of the assembly is represented as

$$E_f^{-1} = \langle \sin^4\xi \rangle (s_{11} - 2s_{13} + s_{33} - s_{44}) + \langle \sin^2\xi \rangle (2s_{13} - 2s_{33} + s_{44}) + s_{33} \tag{39}$$

where

$$\langle \sin^4\xi \rangle = \frac{(\omega + 4)(\omega + 2)}{(\omega + 5)(\omega + 3)} \tag{40}$$

$$\langle \sin^2\xi \rangle = \frac{\omega + 2}{\omega + 3} \tag{41}$$

3.1.4. Series rotatable elements model

Equation 39 represents the relationship between the tangent modulus and the crystallite orientation, but does not describe the relationship between the crystallite orientation and tensile stress. Northolt *et al.* [6] have derived the crystallite orientation as a function of tensile stress from a geometrical consideration on cubic-shaped crystallites. This model by Northolt *et al.* will be called a series rotatable elements model for convenience, and a brief outline of the derivation by using a coordinate transformation is given below.

The series rotatable elements model, shown in Fig. 4, starts from the same assumptions as those adopted for the series elements model. In addition, the rotation angle $d\xi$ of a crystallite due to a small increment of tensile stress $d\sigma_{ff}$ of the assembly is assumed to be equal to the increment of shear strain $d\varepsilon_{13}$ of a crystallite. That is,

$$d\xi = d\varepsilon_{13} = s_{1311} d\sigma_{11} + s_{1333} d\sigma_{33} + s_{1313} d\sigma_{13} + s_{1331} d\sigma_{31} \tag{42}$$

With the crystallites in carbon fibres, the components of the compliance tensor s_{1311} and s_{1333} are zero, and s_{1313} and s_{1331} are one quater those of s_{55} and of s_{44}. In addition, by a coordinate transformation,

$$d\sigma_{13} = d\sigma_{31} = \cos\xi \sin\xi\, d\sigma_{ff} \tag{43}$$

Hence,

$$\frac{d\xi}{\cos\xi \sin\xi} = \frac{1}{2} s_{44}\, d\sigma_{ff} \tag{44}$$

Integrating the above equation and approximating $\tan^2\xi$ with $\cos^{-2}\xi$ leads to

$$\cos^2\xi = \cos^2\xi_0 \exp(-s_{44}\sigma_{ff}) \tag{45}$$

where ξ_o is the initial orientation angle. By averaging $\cos^2\xi$ for all the crystallites,

$$\langle \cos^2\xi \rangle = \langle \cos^2\xi_0 \rangle \exp(-s_{44}\sigma_{ff}) \tag{46}$$

The compliance of a crystallite and of the assembly are given respectively by Equations 38 and 39. By representing $\sin\xi$ in Equation 38 by using $\cos\xi$ and by taking into account that for carbon fibres with a high crystallite orientation, s_{11} and $s_{13} \ll s_{44}$, and $\cos^4\xi \ll \cos^2\xi$, Equation 39 becomes

$$E_f^{-1} = s_{11} + s_{44}\langle \cos^2\xi \rangle = s_{11} + s_{44}\langle \cos^2\xi_0 \rangle \exp(-s_{44}\sigma_{ff}) \tag{47}$$

If the crystallite orientation distribution is represented by Equation 2, $\langle \cos^2\xi \rangle$ is related to the orientation parameter Π as

$$\langle \cos^2\xi \rangle = \frac{1}{3 - \dfrac{\ln 2}{\ln[\sin(\pi\Pi/2)]}} \tag{48}$$

It should be noted that Equation 42 is valid only when the direction with an angle $\pi/4$ against the 1 and 3 axes does not rotate by tensile stress. In this regard, the series rotatable elements model does not take into account the rotational displacement of the 1 and 3 axes which possibly arises in an assembly under tensile stress.

3.1.5. Parallel elements model

In the parallel elements model shown in Fig. 4, the crystallites with a constant length perpendicularly to the fibre axis are combined transversely with a strong bond. So that when the assembly is subjected to a tensile stress, all the crystallites experience the same tensile strain.

Denote the transverse cross-sectional area of an assembly by A, the tensile stress by σ_{ff}, and the tensile strain by ε_{ff}. Then, the tensile force $A\sigma_{ff}$ of the assembly equals the sum of the tensile forces of respective crystallites. Since in a transverse cross-section of the assembly, a fractional area of the crystallites with orientation angles in a range from ξ to $\xi + d\xi$ is given by $2\pi \sin\xi\, g(\xi) A d\xi$, the tensile force of the assembly is expressed as

$$A\sigma_{ff} = \langle A s_{ff}^{-1} \varepsilon_{ff} \rangle \quad (49)$$

and the tangent modulus E_f of the assembly is represented as

$$E_f = \langle s_{ff}^{-1} \rangle \quad (50)$$

where s_{ff} is given by Equation 38. This model implies that considerable stress differences may occur among the crystallites [6].

3.2 Stress applied to crystallites

Carbon fibres include microvoids and unorganized carbons other than the crystallites [15]. Hence, by denoting a correction factor as v, the tensile stress σ measured for carbon fibres may be related to the tensile stress σ_{ff} of the crystallites as,

$$\sigma = v\sigma_{ff} \quad (51)$$

Similarly, the tangent modulus E of carbon fibres is related to the tangent modulus E_f of the crystallites as

$$E = vE_f \quad (52)$$

In the present study, correction factors obtained by two different ways, one being a correction factor v_c determined from X-ray diffraction and the other being a correction factor v_d calculated as the ratio of the fibre density to the crystallite density, will be applied for the mechanical models. The correction factor v_c is a volume fraction of crystallites in carbon fibres, and was determined from the intensity distribution of the 002 X-ray diffraction peak by the method described in a previous paper [15]. The correction factor v_d has been adopted in a number of papers that discuss the mechanical properties of carbon fibres.

The values of v_c and v_d obtained for a series of carbon fibres are shown as a function of Π_0 in Fig. 5.

3.3 Parameters for evaluating models

In order to evaluate the applicability of mechanical models, an average rate of increase in the tangent modulus with tensile stress $\Delta E/\Delta\sigma$ which is defined as

$$\frac{\Delta E}{\Delta\sigma} = \frac{1}{\sigma_r}\int_0^{\sigma_r}\left(\frac{\partial E}{\partial\sigma}\right)d\sigma = \frac{E_r - E_0}{\sigma_r} \quad (53)$$

is introduced. In Equation 53, E_0 and E_r are the tangent moduli at zero tensile stress and at a tensile stress σ_r corresponding to 40% of the tensile strength. Similarly, an average rate of increase in the crystallite orientation with tensile stress $\Delta\Pi/\Delta\sigma$ defined as

$$\frac{\Delta\Pi}{\Delta\sigma} = \frac{1}{\sigma_r}\int_0^{\sigma_r}\left(\frac{\partial\Pi}{\partial\sigma}\right)d\sigma = \frac{\Pi_r - \Pi_0}{\sigma_r} \quad (54)$$

is also introduced, where Π_r is the crystallite orientation at the tensile stress σ_r. These parameters $\Delta E/\Delta\sigma$ and $\Delta\Pi/\Delta\sigma$ are suitable for representing the tangent modulus and crystallite orientation changes in a relatively wide stress range where the stress–strain response is reversible.

In Figs 6 and 7, the tensile strength and the values of $\Delta E/\Delta\sigma$ and $\Delta\Pi/\Delta\sigma$ obtained experimentally for various carbon fibres are plotted against Π_0. The straight line in Fig. 7 represents a regression line with

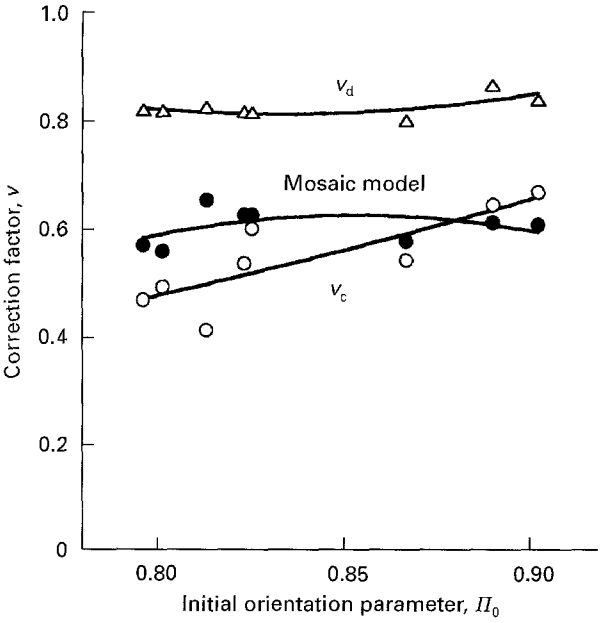

Figure 5 Crystallite volume fraction v_c, ratio of fibre density to crystallite density v_d, and the correction factor determined by mosaic model plotted against initial orientation parameter Π_0.

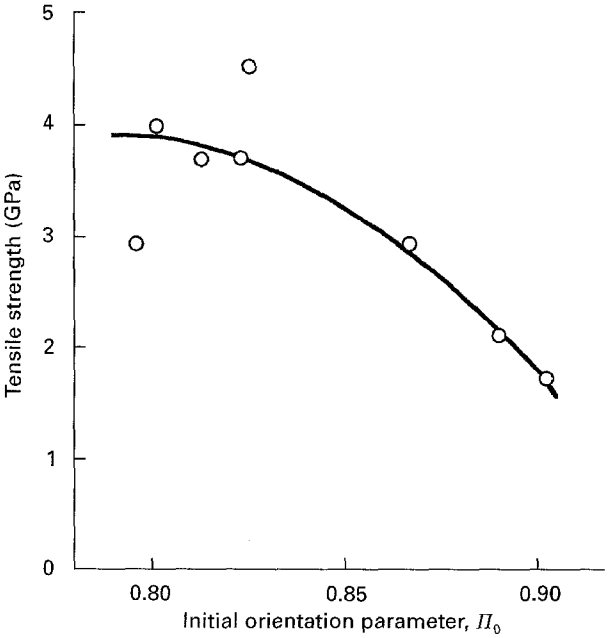

Figure 6 Tensile strength of PAN-based carbon fibres plotted against initial orientation parameter Π_0.

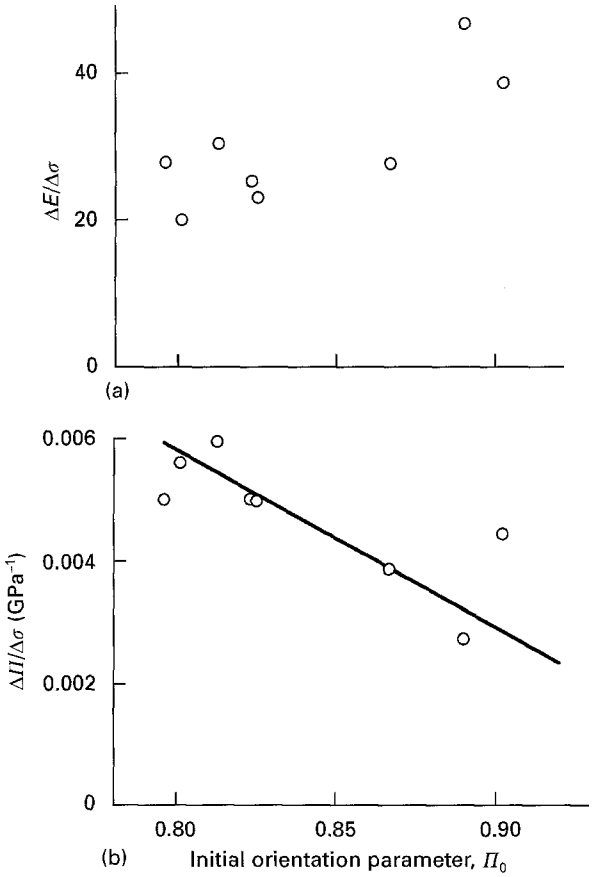

Figure 7 Average rate of increase in tangent modulus with tensile stress $\Delta E/\Delta\sigma$ and in orientation parameter $\Delta\Pi/\Delta\sigma$ plotted against initial orientation parameter Π_0. Regression line with slope 0.030 GPa^{-1} and passing through $(\Pi_0, \Delta\Pi/\Delta\sigma) = (1, 0)$ is shown.

a slope 0.030 GPa^{-1} and passing through the point $(\Pi_0, \Delta\Pi/\Delta\sigma) = (1, 0)$.

3.4 Calculation of one-dimensional array models

3.4.1 Undulating ribbon model

The tangent moduli E_r and E_0 for the undulating ribbon model were calculated by Equation 22 using experimental values of Π_0 and Π_r. For the purpose of studying the applicability of this model to experimental results, the ratio of E_r/E_0 rather than the parameter $\Delta E/\Delta\sigma$ is suitable, since the compliance s_{11} is eliminated from E_r/E_0, as known from Equation 22. The value of E_r/E_0 calculated by using Equation 22 is a function of L_0/h and becomes larger with increasing L_0/h. However, the changes in E_r/E_0 with L_0/h larger than 100 is less than 0.1%. Thus, an infinitely large value was assumed for L_0/h.

3.4.2 Zigzag ribbon model

With the zigzag ribbon model, the expressions relating the tangent modulus and the crystallite orientation to the tensile stress given by Equations 31 and 35 involve two compliances s_{11} and r_{55}. The compliance r_{55} was determined so that the value of Π_r calculated by Equation 35 using an experimental value of Π_0 was consistent with the experimental result. Then s_{11} was determined at a value which makes the value of E_0, calculated by Equation 31 using the value of r_{55}, consistent with the experimental result. By using the values of s_{11} and r_{55} as determined above, E_r was calculated by Equation 31, and the value of $\Delta E/\Delta\sigma$ was obtained.

TABLE I Components of compliance matrix, s_{ij}, and stiffness matrix, c_{ij}, for graphite

Compliance (GPa^{-1})		Stiffness (GPa)	
s_{11}	9.8×10^{-4}	c_{11}	1060
s_{12}	-1.6×10^{-4}	c_{12}	180
s_{13}	-3.3×10^{-4}	c_{13}	15
s_{33}	2.8×10^{-2}	c_{33}	37
s_{44}	5.6~2.9	c_{44}	0.18~0.35

3.4.3 Series elements model

In Equation 39 representing the tangent modulus versus crystallite orientation for the series elements model, the compliance s_{44} is assumed as an adjustable parameter. For the compliances s_{11}, s_{13} and s_{33}, the compliances for graphite listed in Table I [19] were used. The compliance s_{44} was determined at a value which makes the value of E_0, calculated by Equation 39 using an experimental value of Π_0, consistent with the experimental result. Then the parameter $\Delta E/\Delta\sigma$ was calculated by Equation 39 using the compliances s_{11}, s_{13}, s_{33} and s_{44}, and an experimental value of Π_r.

3.4.4 Series rotatable elements model

The tangent modulus and the crystallite orientation versus tensile stress relations for the series rotatable elements model represented by Equations 46 and 47 involve two compliances s_{11} and s_{44}. The compliance s_{44} was determined by Equation 46 using experimental values of Π_0 and Π_r. Then the compliance s_{11} was determined by Equation 47 using the value of s_{44} and experimentally obtained E_0. The parameter $\Delta E/\Delta\sigma$ was calculated by Equation 47 using s_{11} and s_{44} thus determined.

3.4.5 Parallel elements model

The parallel elements model represented by Equation 50 involves four compliances s_{11}, s_{13}, s_{33} and s_{44}. For the compliances s_{11}, s_{13} and s_{33} the values of graphite were used. The compliance s_{44} was determined by Equation 50 using experimental values of E_0 and Π_0. Then using this value of s_{44} and experimentally obtained Π_r the parameter $\Delta E/\Delta\sigma$ was calculated by Equation 50.

3.5 Comparison with experimental results

In Fig. 8, the values of E_r/E_0 calculated by the undulating ribbon model are compared with the experimental values. Fig. 8 indicates that this model gives considerably smaller values of E_r/E_0 than the experimental values.

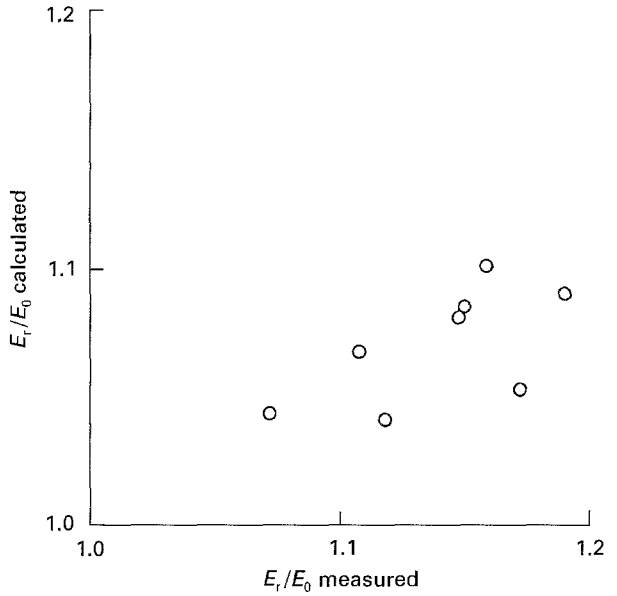

Figure 8 Ratio of tangent modulus at 40% of tensile strength to that at zero stress calculated by undulating ribbon model plotted against experimental values. L_0/h was taken to be infinitely large.

Values of the compliances of the zigzag ribbon, series elements, series rotatable elements, and parallel elements models calculated using v_c and v_d are shown in Table II. In Fig. 9 the $\Delta E/\Delta\sigma$ values calculated by these models using v_c and v_d are compared with the experimental results. As is shown in Fig. 9, the $\Delta E/\Delta\sigma$ values calculated with the models are considerably smaller than the experimental values. The difference between the calculated and experimental values is scarcely affected by the magnitude of the correction factors.

It should be concluded, therefore, that the one-dimensional array models cannot represent the non-hookean stress–strain response of carbon fibres associated with the crystallite orientation changes with tensile stress.

4. Mosaic model for non-hookean stress–strain response with orientation changes

From the above analysis, it is clear that in order to explain the increase in the tangent modulus with tensile stress for carbon fibres, a mechanism that constrains the deformation of the crystallites with increasing tensile stress, in addition to the mechanism of increasing the crystallite orientation, is required. For this purpose, a model which will be called a mosaic model henceforth is proposed and its validity is discussed in the following subsections.

4.1 Constitution of mosaic model

In the mosaic model shown in Fig. 4, it is assumed that the equidimensional cubic crystallites are arranged in a two dimensional array forming a hexahedral assembly. The deformation of this assembly subjected to a tensile force is analysed by a finite element method (FEM).

In the assembly, $16 \times 16 \times 1$ crystallites are arranged in the longitudinal, the transverse and the thickness directions respectively where the longitudinal direction is defined as being parallel to the fibre axis. We denote the vectors defining three neighbouring edges of a crystallite in the longitudinal, the transverse and the thickness directions as $\boldsymbol{X}_i$, $\boldsymbol{Y}_i$ and $\boldsymbol{Z}_i$, respectively. In a continuous distribution of orientation angle ξ, which is measured without applying a tensile stress to the fibres, a range of ξ where the layer normals mainly populate is divided into 15 sections. Then

TABLE II Compliances in GPa^{-1} units of zigzag ribbon, series elements, series rotatable elements and parallel elements models calculated with v_c and v_d.

Π_0	Zigzag ribbon		Series elements	Series rotatable elements		Parallel elements
	s_{11}	r_{55}	s_{44}	s_{11}	s_{44}	s_{44}
Calculated with v_c						
0.7960	0.0018	0.011	0.026	0.0013	0.020	0.083
0.8011	0.0015	0.013	0.024	0.00089	0.024	0.073
0.8129	0.0011	0.013	0.015	0.00052	0.023	0.035
0.8231	0.0014	0.015	0.026	0.00080	0.027	0.070
0.8251	0.0015	0.017	0.031	0.00083	0.031	0.089
0.8667	0.0014	0.015	0.031	0.00095	0.030	0.071
0.8900	0.0016	0.016	0.052	0.0013	0.031	0.13
0.9022	0.0015	0.021	0.055	0.0011	0.041	0.13
Calculated with v_d						
0.7960	0.0031	0.019	0.062	0.0022	0.034	0.33
0.8011	0.0025	0.022	0.055	0.0015	0.040	0.26
0.8129	0.0021	0.025	0.054	0.0010	0.046	0.24
0.8231	0.0021	0.022	0.052	0.0012	0.041	0.21
0.8251	0.0020	0.022	0.050	0.0011	0.042	0.20
0.8667	0.0020	0.023	0.064	0.0014	0.044	0.22
0.8900	0.0022	0.021	0.087	0.0018	0.041	0.30
0.9022	0.0018	0.027	0.085	0.0014	0.052	0.25

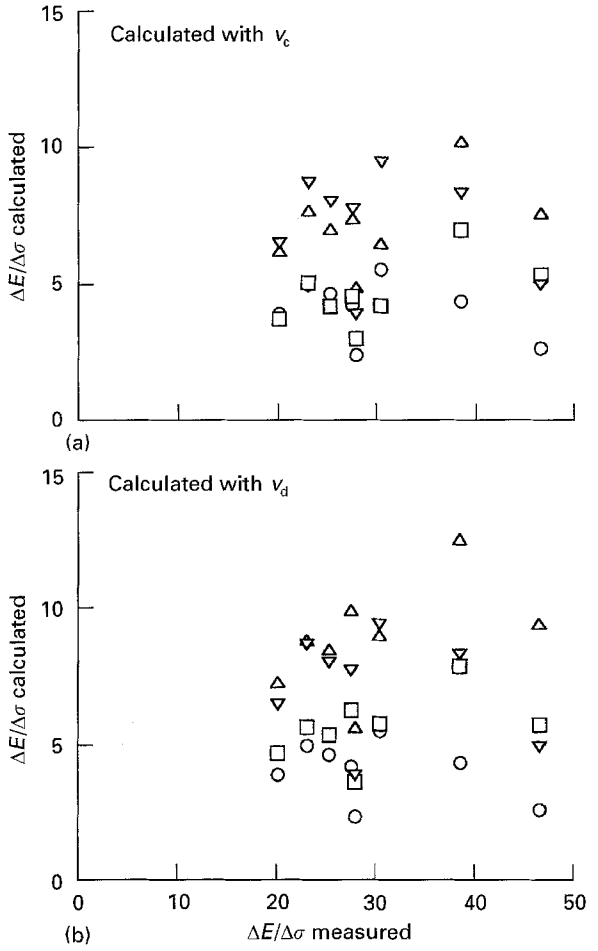

Figure 9 Average rate of increase in tangent modulus with tensile stress $\Delta E/\Delta\sigma$ calculated by; (○) zigzag ribbon, (△) series elements, (▽) series rotatable elements and (□) parallel elements models plotted against experimental values. Volume fraction of crystallites v_c and ratio of fibre density to crystallite density v_d were used as correction factor v.

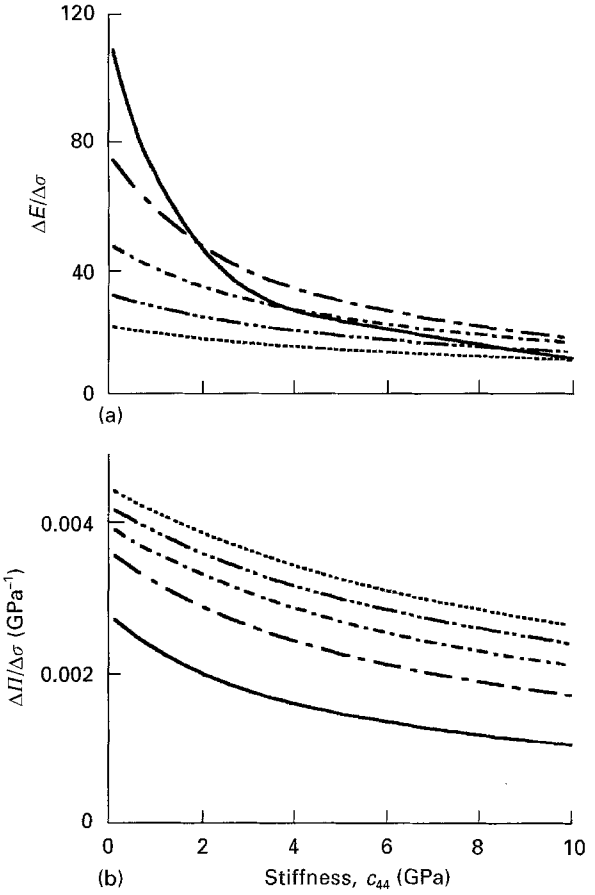

Figure 10 Average rate of increase in tangent modulus with tensile stress $\Delta E/\Delta\sigma$ and in orientation parameter $\Delta\Pi/\Delta\sigma$ calculated by the mosaic model plotted against stiffness c_{44}. Correction factor v was taken to be unity. The values of Π_0 used were (- - - -) 0.75, (— - -) 0.80, (- · - ·) 0.85, (— - — -) 0.90 and (——) 0.95.

a discrete orientation distribution whose $\langle\cos^2\xi\rangle$ value is consistent with the experimental value is obtained. The discrete orientation distribution obtained thus is arranged to 256 crystallites in a random manner. A stiffness matrix of a crystallite with orientation angle ξ is obtained from the stiffness matrix produced from the principal axes of the crystallite by a coordinate transformation. This coordinate transformation is made by rotating a principal axis parallel to the layer normal by an angle ξ against the $\boldsymbol{X}_i$ vector in the $\boldsymbol{X}_i - \boldsymbol{Y}_i$ plane. The vector $\boldsymbol{X}_i$ for the initial state of the assembly before deformation is parallel to the fibre axis. When the assembly is subjected to a tensile force, the $\boldsymbol{X}_i$, $\boldsymbol{Y}_i$ and $\boldsymbol{Z}_i$ vectors rotate and are no longer in general orthogonal after deformation. The rotation angle of the carbon layer due to the tensile force is defined as the angle made between the fibre axis and the $\boldsymbol{X}_i$ vector after deformation.

In the FEM calculation, a multiple point constraint is applied to the nodes on the contour of the assembly so that the four sides of the assembly parallel to the thickness displace, keeping the planarity, according to tensile force.

The trajectory of the $\boldsymbol{X}_i$, $\boldsymbol{Y}_i$ and $\boldsymbol{Z}_i$ vectors during deformation is calculated by a so-called update Lagrange method. That is, by applying a small extension to the initial state of the assembly, the resultant tensile force of the assembly and the rotation angles of respective crystallites are calculated. Then, as the second extension, a small extension is further applied to the deformed assembly, and the resultant tensile force and the rotation angles are calculated. The sum of the tensile forces and of the rotation angles for the first and the second extensions are the tensile force and the rotation angles yielded by the extension from the initial state to the second extension. These procedures are iterated until the required extension is achieved. The tangent modulus is calculated from the increase in extension and in tensile force at each step. The orientation parameter is calculated by Equation 48 using the $\langle\cos^2\xi\rangle$ value of the 256 crystallites.

4.2. Application of mosaic model

In applying the mosaic model to experimental results, the correction factor v and the stiffness c_{44} were assumed to vary amongst different types of carbon fibres. For the stiffnesses other than c_{44}, the values for graphite were adopted. The changes of $\Delta E/\Delta\sigma$ and $\Delta\Pi/\Delta\sigma$ with c_{44} calculated by the mosaic model using $v = 1$ and various values of Π_0 are shown in Fig. 10. It can be seen from Fig. 10 that in comparison with $\Delta\Pi/\Delta\sigma$ the changes of $\Delta E/\Delta\sigma$ with c_{44} are easy to detect. Hence, when determining a value of c_{44}, it is

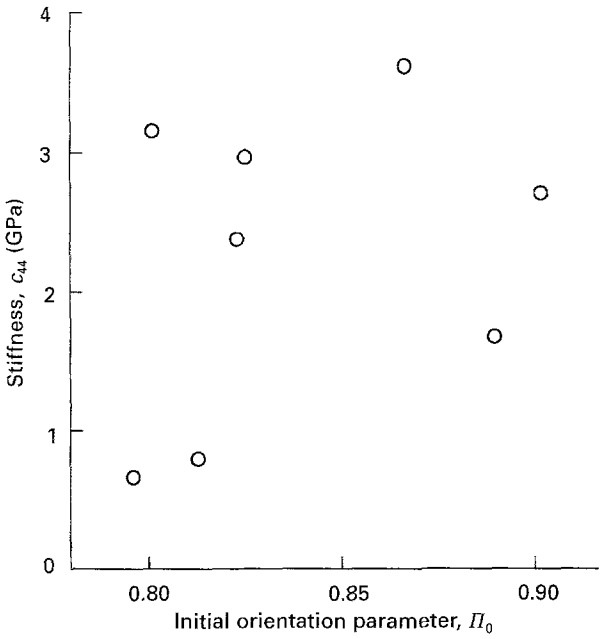

Figure 11 Stiffness c_{44} calculated by the mosaic model plotted against initial orientation parameter Π_0.

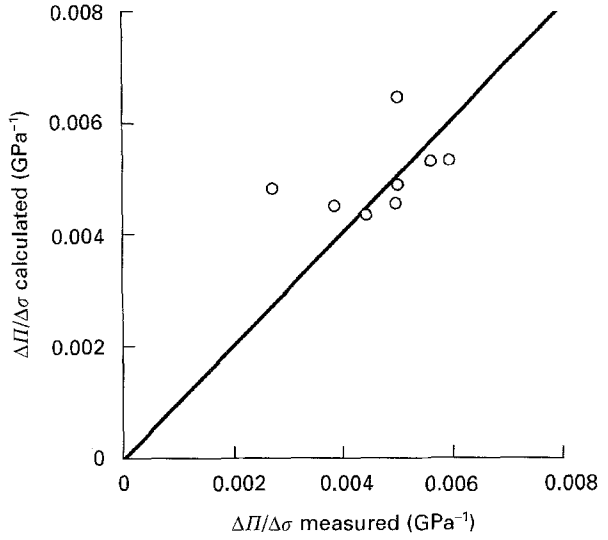

Figure 12 Average rate of increase in orientation parameter with tensile stress $\Delta\Pi/\Delta\sigma$ calculated by the mosaic model plotted against experimental values.

preferable to utilize the $\Delta E/\Delta\sigma$ versus c_{44} relation in order to minimize any possible error.

Values of v and c_{44} for carbon fibres were determined by the following procedure. Firstly, by assuming a value of c_{44}, v was obtained so that a value of E_0, calculated using an experimental value of Π_0, coincided with the experimental result. Secondly, the tensile stress σ_r was calculated using the value of v and the tensile strength of the fibre. Thirdly, the parameter $\Delta E/\Delta\sigma$ was calculated by using σ_r, v and the assumed value of c_{44}. Fourthly, by changing the value of c_{44} and iterating similar calculations, the relation between c_{44} and $\Delta E/\Delta\sigma$ was obtained. Finally, the values of c_{44} and v were determined at the values which gave $\Delta E/\Delta\sigma$ consistent with the experimental result.

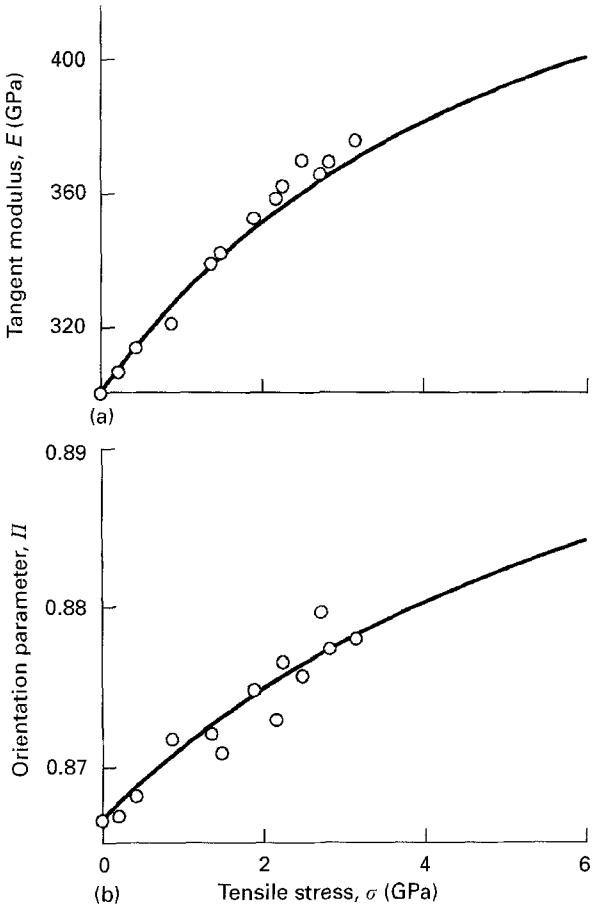

Figure 13 Tangent modulus E and orientation parameter Π of a carbon fibre with initial orientation parameter 0.867 plotted against tensile stress σ of fibre. Curves were calculated by the mosaic model.

The values of v and c_{44} obtained for various carbon fibres are plotted against Π_0 in Figs 5 and 11, respectively. Fig. 5 indicates that the correction factor calculated from the mosaic model gives a value closer to the crystallite volume fraction v_c rather than the density ratio v_d. It has been reported that in the case of graphite the stiffness c_{44} differs according to preparation conditions of graphite and shows various values in a range from 0.1–5 GPa [6]. In Fig. 11 the values of c_{44} are distributed in a range similar to that reported for graphite and their average is about 3 GPa. In Fig. 12 the $\Delta\Pi/\Delta\sigma$ values calculated by the mosaic model are plotted against the experimental values. The calculated values are in good agreement with the experimental values.

In Fig. 13 typical examples of mosaic model calculations on the changes of the tangent modulus and the crystallite orientation with tensile stress are shown together with the measured values. It is noted that the mosaic model closely predicts the parabolic nature observed experimentally in those relations.

5. Conclusion

Amongst various one-dimensional array models and a mosaic model, only the mosaic model gave a quantitative agreement with the measured increases in the tensile modulus and the crystallite orientation with tensile stress. The parabolic nature found in those

relations was also predicted by the mosaic model. This suggested that the deformation of the crystallites is constrained with increasing tensile stress. It was also found that the ratio of the tensile stress of the fibre to that of the crystallites is close to the crystallite volume fraction rather than the ratio of the fibre density to the crystallite density.

References

1. G. J. CURTIS, J. M. MILNE and W. N. REYNOLDS, *Nature* **220** (1968) 1024.
2. C. P. BEETZ, *Fibre Sci. Technol.* **16** (1982) 219.
3. C. P. BEETZ and G. W. BUDD, *Rev. Sci. Instrum.* **54** (1983) 1222.
4. I. M. KOWALSKI, Eight Conference, "Composite Materials: Testing and Design" *ASTM STP* 972 (American Society for Testing and Materials, Philadelphia, PA 1988) p. 205.
5. Y. NUKUSHINA, J. MATSUI and M. ITOH, *J. Jpn Soc. Composite Mater.* **15** (1989) 210.
6. M. G. NORTHOLT, L. H. VELDHUIZEN and H. JANSEN, *Carbon* **29** (1991) 1267.
7. W. H. M. VAN DREUMEL and J. L. M. KAMP, *J. Composite Mater.* **11** (1977) 461.
8. T. ISHIKAWA, M. MATSUSHIMA and Y. HAYASHI, *J. Mater. Sci.* **20** (1985) 4075.
9. H. VANGERKO and A. J. BARKER, *Composites* **16** (1985) 19.
10. J. D. H. HUGHES, *Carbon* **24** (1986) 551.
11. M. M. STEVANOVIC and T. B. STECENKO, *J. Serb. Chem. Soc.* **57** (1992) 785.
12. E. HAYAKAWA, M. SHIOYA and A. TAKAKU, *Adv. Composite Mater.* **4** (1994) 33.
13. T. B. STECENKO and M. M. STEVANOVIC, *J. Composite Mater.* **24** (1990) 1152.
14. P. ARSENOVIC, H. JIANG, R. K. EBY, W. W. ADAMS and J. M. LIN, in Proceedings Carbon 88, University of Newcastle upon Tyne, UK, edited by B. McEnaney and T. J. Mays (Institute of Physics, 1988) p. 485.
15. A. TAKAKU and M. SHIOYA, *J. Mater. Sci.* **25** (1990) 4873.
16. M. SHIOYA and A. TAKAKU, *Carbon* **32** (1994) 615.
17. W. RULAND, *Appl. Polym. Symposia* **9** (1969) 293.
18. M. STEWART and M. FEUGHELMAN, *J. Mater. Sci.* **8** (1973) 1119.
19. O. L. BLAKSLEE, D. G. PROCTOR, E. J. SELDIN, G. B. SPENCE and T. WENG, *J. Appl. Phys.* **41** (1970) 3373.

Received 2 October 1995
and accepted 18 March 1996